Optimization of Chitosan-PEG/ZnO Hydrogel Formulation with Pomegranate Peel Extract as an Alternative for Wound Healing

Niamul Faza Assauqi¹, Retno Ariadi Lusiana^{1*}, and Nanang Masruchin²

¹Department of Chemistry, Faculty of Science and Mathematics, Diponegoro University, Jl. Prof. Soedharto SH, Tembalang, Semarang 50275, Indonesia

²Research Center for Biomass and Bioproducts, National Research and Innovation Agency (BRIN), KST Soekarno, Cibinong 16911, Indonesia

* Corresponding author:

email: retno.lusiana@live.undip.ac.id

Received: March 6, 2025 Accepted: April 12, 2025

DOI: 10.22146/ijc.105215

Abstract: A chitosan-zinc oxide (ZnO)/poly(ethylene glycol) (PEG)/pomegranate peel extract (PE) based hydrogel has been developed as a potential material to accelerate the wound healing process by controlling the drug release mechanism. ZnO nanoparticles with an average size of about 95 nm were synthesized using the co-precipitation method and then combined into chitosan/PEG composites to improve the antimicrobial properties of the hydrogels. Characterization of the hydrogels included analysis of size, morphology, elemental composition, microstructure, swelling behavior, antibacterial activity, and wound healing effectiveness. The results of the in vitro study indicated that the antibacterial activity of PE-containing hydrogel against Escherichia coli and Staphylococcus aureus decreased due to the chelation effect caused by PE addition. However, in vivo tests for 10 d showed that the PE-containing hydrogel had better wound healing ability than commercial betadine. In addition, the developed hydrogel showed high biocompatibility with excellent antibacterial activity. This study confirmed that chitosan/PEG/ZnO nanoparticle hydrogel has the potential as wound dressing materials with sustained drug release and optimal healing effectiveness.

Keywords: hydrogel; chitosan; pomegranate peel extract; ZnO; wound healing

■ INTRODUCTION

The skin is the body's first defense organ and has a high self-healing potential. However, when there is a dangerous open wound, the natural wound healing process likely takes a long time, resulting in a dangerous situation. Therefore, tissue repair adjuvants in the proliferation phase are needed to accelerate the wound healing process [1]. Natural polymers like chitosan (Cs) are biodegradable, biocompatible, and odorless, and they have antibacterial activity, low immunogenicity, and enhance interactions with polymer cells, improving cell proliferation [2-5]. Cs is a linear polysaccharide that is soluble only in acidic solutions derived from the deacetylation of chitin. It is extensively utilized in biomedical applications, including wound dressings [6]. Cs contains several -NH2 and -OH groups, which are easily substituted with other functional groups for specific purposes [7-9]. Masud et al. [7] developed Cs-based hydrogels with the addition of ZnO and gentamicin into hydrogels in *in vitro* analysis, showing an increase in antibacterial activity of drugcontaining bionanocomposites on *Escherichia coli* and *Salmonella enterica* due to the combined effect of gentamicin and ZnO nanoparticles (ZnO-NP). Hosseini et al. [8] developed BA-PEG Cs-based hydrogels with the addition of graphene oxide nanoparticles and pomegranate peel, resulting in antimicrobial activity reaching 99%.

Although Cs are extensively utilized in medical applications, like most natural polymers, they have limited mechanical properties [10-11]. To improve its applicability, Cs are usually combined with other polymers [10,12-14]. Polyethylene glycol (PEG) is one polymer that can be blended with Cs to enhance biocompatibility, hydrophilicity, and mechanical

strength. PEG was chosen to prepare wound dressings because it is biocompatible, non-toxic, hydrophilic, flexible, and non-immunogenic [15]. PEG is a highly water-soluble synthetic polymer with a similar chemical structure as a primary hydroxyl group at the end of a polyether chain containing oxyethylene (CH₂–CH₂–O). PEG is widely used in the food, cosmetic, and pharmaceutical industries. Crosslinking between Cs and PEG can be acquired using crosslinking agents like sodium tripolyphosphate (STPP) [16]. A crosslinked structure with increased chemical stability and flexibility is produced when specific phosphate groups in STPP come into contact with the protonated amino groups of Cs and the hydroxyl groups of PEG [7].

In recent years, Cs modified into a hydrogel form have been considered a promising candidate for improving wound healing because they are highly stable, protect the wound from infection, and maintain a moist environment [17]. Coupled with incorporating various nanoparticles, such as ZnO, as an antibacterial agent to prevent infection. ZnO-NP have desirable properties, including antibacterial activity, high surface area, nontoxicity, photocatalytic activity, and anticancer [18-20]. Zn protects cells against reactive oxygen species and bacterial toxins through its antioxidant activity, and it has been observed that delayed wound healing is caused by Zn deficiency in the diet or hereditary reasons [21-22].

In addition, herbal extracts have been utilized as natural alternatives and as a sustainable for chemical drugs for tissue regeneration [23]. Pomegranate peel extract (PE) is among the potent natural medicinal materials, consisting of beneficial compounds, including tannins, alkaloids, flavonoids, phenolic acids, steroids, vitamins, and minerals. Appealingly, the concentration of these compounds is generally higher in pomegranate peel than in the fruit itself. It is important to highlight that the synergistic interaction of these active components in PE can result in various effects, like antioxidant, antiinflammatory, and antibacterial properties [24-26]. This study studied the preparation of Cs-based hydrogels and the potential to accelerate the wound healing process. Hydrogels based on Cs-PEG/ZnO and PE were studied to elucidate antibacterial and promote healing of infectious wounds. Chemical structure, swelling ratio, drug release, antibacterial activity and wound healing effect were evaluated *in vitro* and *in vivo*.

EXPERIMENTAL SECTION

Materials

Chitosan (Chimultiguna lab, DD = 87.00%), PEG (Merck, Mw = 4000.00 g/mol), Zn(CH₃COO)₂·2H₂O (Merck), Chloroform (Merck), STPP (Sigma Aldrich), NH₄OH (Merck), NaOH (Merck), HCl (Merck), CH₃COOH (Merck), EtOH (Merck), Mueller Hinton Agar (MHA, oxoid), and Nutrient Broth (NB, Merck) were used in this study.

Instrumentation

FTIR (PerkinElmer Spectrum IR), DLS (NanoPartica SZ-100V2), XRD (Shimadzu MaximaX-Scientific 7000), SEM (Thermo Quattro spectrophotometer UV-vis (PG Instruments), oven (Memmert), hot plate Stirrer (FAITHFUL), analytical balance (OHAUS), laminar airflow (LAF,FAITHFUL), incubator (Memmert), shaker (DLAB sk-1080-s), and centrifuge (Hettich Zentrifugen EBA 200) were used in this study.

Procedure

Synthesis of ZnO-NP

ZnO-NP was synthesized using the coprecipitation approach described by Purwaningsih et al. [27] with minor adjustments. To make a 50 mL of Zn(CH₃COO)₂, a 0.5 M HCl solution was used to dissolve 5.487 g of Zn(CH₃COO)₂·2H₂O. Then, 0.5 M NH₄OH solution was added dropwise to the prior solution at 85 °C while being constantly stirred until the pH of the mixture reached 9. For 5 h. The solution was continuously stirred at 85 °C in order to get the required ZnO size. Next, ZnO-NP was separated using a centrifuge at 6,000 rpm for 15 min, followed by washing using deionized water to remove impurities. Once clean, ZnO was calcined at 400 °C for 2 h.

Preparation of PE

Pomegranate peel powder was purchased from Indoplant Herbs, Indonesia, and was extracted with the

maceration method using 70% ethanol in a ratio of 1:10. A total of 25 g of pomegranate peel powder was dissolved in 250 mL of 70% ethanol. The extract was allowed to stand for 3 d while occasionally stirring to dissolve the active compounds. The extract was then filtered and concentrated by a rotary evaporator at 50 °C. The result of liquid PE is stored in amber glass and in the refrigerator [28-29].

Preparation of nanocomposite hydrogel

PEG and ZnO modified Cs hydrogels were prepared using a combined method from previous works [7,30-31]. The composition of the hydrogel variation is shown in Table 1. A total of 500 mg Cs was dissolved in 40 mL of 1% (v/v) acetic acid and 125 mg PEG was added while stirring continuously until a homogeneous solution was obtained. At the same time, a stoichiometric amount of ZnO was dissolved in 10 mL of 1% (v/v) acetic acid. Both solutions were mixed and 3 mL of 0.5% STTP solution was added. Stirring was continued for 4 h with a temperature range of 60-80 °C. PE was added to the produced hydrogel solution at a concentration of 20 mg/mL (crude PE dissolved in acetic acid 1%/PEG solution). Then, 1 M NaOH solution was gradually added until a white precipitate formed. Centrifugation at 5,000 rpm for 10 min was used to separate the precipitate, then aquadest was washed until the pH solution reached 7. To obtain the final bionanocomposite, freeze-drying was used.

Drug loading

Before the gelation procedure, PE was added to the produced hydrogel solution at a 20 mg/mL concentration. Using UV-vis spectroscopy at a wavelength of 273 nm, drug loading (DL) and encapsulation efficiency (EE) were

measured and computed using Eq. (1) and (2) [8].

$$DL(\%) = \frac{\text{Weight of PE in the hydrogel}}{\text{Weight of hydrogel}} \times 100\%$$
 (1)

$$EE(\%) = \frac{Actual loading}{Theoretical loading} \times 100\%$$
 (2)

Characterization techniques

FTIR analysis was carried out on Cs/PEG-based hydrogels within the 400–4000 cm⁻¹ range. The crystal size of ZnO-NP was measured using a XRD with CuK radiation. It operated between 10 and 80° with an angle of diffraction (20) range and scanning speed of 5°/min. In order to improve aggregation identification and measurement of small particles, the diameter of ZnO-NP was measured utilizing dynamic light scattering (DLS) with a performance two-angle particle and molecular size analyzer. Z-potential analysis was also used to ascertain the stability of the ZnO solution. SEM was used to examine the hydrogel morphology.

Swelling test

The procedure was described by Masud et al. [7]. PBS solution (pH 7.4) was prepared for the swelling test. First, the hydrogel was cut into the same size (2×2 cm) and weighed (Wd). Then it was dipped in buffer and put into an incubator at 37 °C. At specific time intervals of 0.5, 1, 2, 4, 24, and 48 h, the hydrogel was taken out of the container, and the surface solution was carefully blotted with tissue paper to remove water from the surface. The Eq. (3) calculates the swelling ratio:

Swelling ratio(%) =
$$\frac{W_s - W_d}{W_d} \times 100\%$$
 (3)

where W_d is the name for the weight of the dry film sample, and W_s is the weight of the swollen film sample. The experiment was conducted in duplo.

Table 1. Differentiation of hydrogel formulation

Code	Hydrogel	Chitosan (mg)	PEG (mg)	STPP (mg)	ZnO (mg)	PE (mg/mL)
F1	Cs/PEG	500	125	15	-	_
F2	Cs/PEG/ZnO1	500	125	15	10	-
F3	Cs/PEG/ZnO4	500	125	15	40	-
F4	Cs/PEG/ZnO1/PE	500	125	15	10	20
F5	Cs/PEG/ZnO4/PE	500	125	15	40	20

Drug release study

The procedure described by Wang et al. [32] as followed in the *in vitro* drug release tests. ZnO/PE-containing hydrogel samples measuring 1.5×1.5 cm were put in an Erlenmeyer with 100 mL of PBS at pH 7.4 and shaken in an orbital shaker set to 37 °C. An amount of 1 mL of buffer was taken out and replaced with an equivalent volume of fresh buffer at the prearranged interval. The amount of released medication in the buffer was determined by measuring the absorbance at 237 nm.

Antibacterial activity

The disc diffusion method was used to examine the prepared materials' antibacterial qualities. Gram-positive *Staphylococcus aureus* and Gram-negative *E. coli* bacteria were cultivated in NB medium at 37 °C until the suspension turbidity matched that of the Mc Farland 0.5 standard solution (roughly 1.5×10^8 bacteria per milliliter of this suspension). MHA was filled with the prepared bacterial suspension ($100~\mu L$), and the mixture was then leveled. The 10~mm-diameter hydrogel was put inside a cup with each bacterium. To identify the zone of inhibition, the plates were subsequently incubated in an incubator for 24~h at 37~°C.

In vivo analysis

Animal administration. Male Wistar rats weighing between 150 and 250 g were used to analyze the effectiveness of hydrogel wound healing in vivo test. All treatments involving animals were approved by Diponegoro University's Institutional Animal Ethics Committee, and the research methodology was carried out in accordance with the European Community's norms and established criteria for the use of laboratory animals. Wistar rats were given a standard diet consisting of water and pellets. Throughout the trial, the rats were housed in a controlled setting with a 12-h cycle of light and dark. To get them unconscious, they were sedated with chloroform for around 3 min [33]. The appropriate wound area was demarcated in the interscapular region, approximately 5 mm from the ears, and their dorsal fur was shaved with a trimmer. Using a punch biopsy, a 6 mm diameter wound was made, guaranteeing that all epidermal and dermal layers were removed to generate a full-thickness wound with the least bleeding [34].

Skin wound healing. The healing activity of the wound area was evaluated by wound excision in a rat model. Wistar rats (150–250 g, 3 months old) were selected for the experiment. They were anesthetized using chloroform [33]. Their dorsal fur was shaved using a trimmer. After the rats lost consciousness, an excision wound was made on the dorsal skin of the rats using a 6 mm diameter biopsy punch, thereby creating a chronic wound [34]. The wound was treated with a 1.5×1.5 cm hydrogel sheet, and 10% povidone iodine was used as a control. The procedure was performed twice for each treatment with a similar wound size [7]. A gradual reduction in wound size was observed, with photographs taken at regular intervals. Wound healing efficiency (HE) was measured using Eq. (4).

Healing efficiency(%) =
$$\frac{\text{Total healed area}}{\text{Total wound area}} \times 100\%$$
 (4)

■ RESULTS AND DISCUSSION

XRD

The results of XRD analysis on ZnO samples showed the presence of diffraction peaks at several 2θ angles, including around 31.52° (100), 34.16° (002), 35.68° (101), 47.19° (102), 56.2° (110), 62.56° (103), 67.05° (112), and 81.02° (202). The diffractogram of the sample obtained in Fig. 1(a) shows a narrow peak. Narrower peaks affect the particle size and consequently the particles become larger [27]. This diffraction pattern matches the hexagonal wurtzite ZnO crystal structure based on JCPDS reference data No. 36-1451. The diffraction peak with the highest intensity is located in the (101) plane, which is characteristic of ZnO with a wurtzite structure [35]. The presence of sharp and welldefined peaks indicates that ZnO has a high degree of crystallinity. In addition, diffraction peaks associated with impurity phases such as Zn, Zn(OH)2, or ZnO2 were not observed in the XRD patterns, indicating the high purity of the synthesized product. These results are in agreement with other reports in the literature. Babayevska et al. [36] study on the structure of ZnO shows that the resulting structure is wurtzite because it is characterized by typical ZnO peaks with wurtzite structure in the (101) plane.

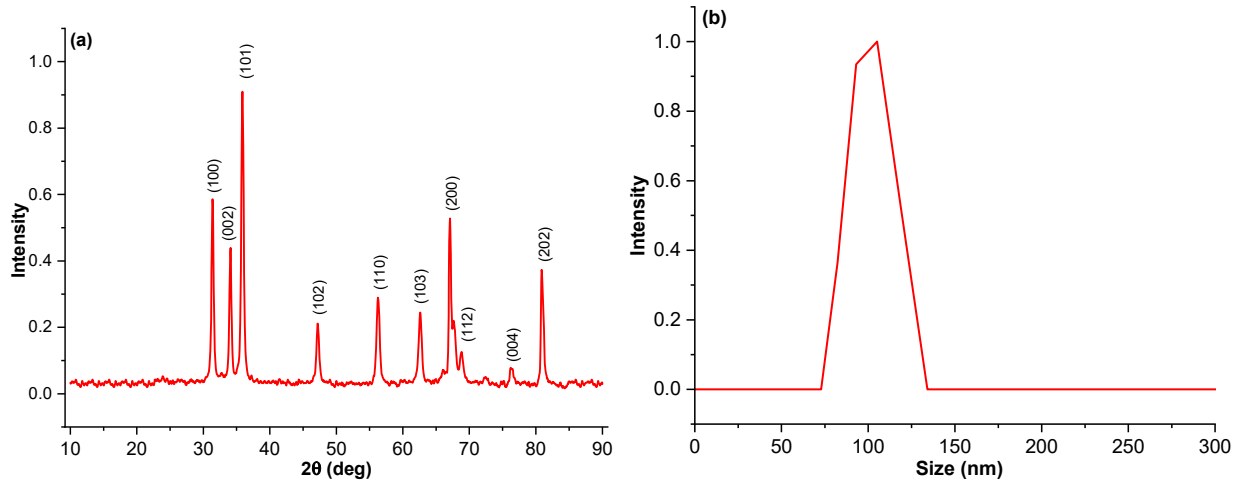


Fig 1. (a) XRD Spectrum of ZnO-NP and (b) the size of ZnO-NP obtained by dynamic light scattering

DLS

The synthesis of ZnO-NP was obtained through the co-precipitation method to produce nano-sized ZnO particles. Based on Fig. 1(b), the size distribution of ZnO-NP looks uniform, with an average hydrodynamic diameter of 95.0 nm. The larger surface area has a significant impact on antibacterial performance. This is in line with research conducted by Babayevska et al. [36], where the smaller the diameter of ZnO, the greater the antibacterial activity, because small particles have a larger surface area to interact with microorganisms. In addition, zeta potential analysis showed a value of -44 mV (SI), which indicates that ZnO-NP has a significant negative surface charge and good colloidal stability. A zeta potential value above ±30 mV indicates that the particles do not agglomerate and can be dispersed evenly in a liquid medium [37]. The combination of small particle size and high stability means that ZnO-NP can be dispersed evenly in hydrogels [38]

Morphology

The micrographs of the hydrogel were analyzed by FESEM as displayed in Fig. 2. The image reveals the semi-porous structure of the hydrogel. The addition of ZnO nanomaterials causes a slight increase in the pore diameter of the hydrogel. Even increasing the content of ZnO-NP in it can cause a decreased amount of crosslinking in the polymer network, creating microscopic walls in the hydrogel's porous structure [39].

Cell and nutrient transport is facilitated by hydrogel scaffolds with linked pores and a suitable pore size. Therefore, scaffolds with pores ranging from 100–500 µm have been proposed as the best substrate for angiogenesis, cell seeding, and the delivery of nutrients and growth factors into the surrounding tissue and structure [40]. Consequently, because these hole diameters are appropriate for promoting cell growth and proliferation, the produced nanocomposite hydrogels can facilitate cell infiltration and migration.

FTIR Study

The FTIR spectra of the hydrogels are shown in Fig. 3(a) and 3(b). Based on Fig. 3(a), peaks were found that the two absorptions located at 564 and 492 cm⁻¹ refer to the vibrational modes of deformation and stretching of the Zn-O bond. In Cs, the observed peaks were 3289 (O-H stretch overlapping with primary N-H), 2897 (C-H stretch of CH₂ symmetry), 1645 and 1585 (amine twin groups), 1376 (asymmetric C-H of CH₂), and 1029 (C-O-C) cm⁻¹ [7]. In the PEG spectrum, peaks were observed at 2881 (C-H strain), 1645 (C=O stretching), 1466 and 1340 (C-H bond deformation vibration), and 1097 (C-O-C bond stretching vibration which is characteristic of PEG) cm⁻¹ [41]. In F1 and F2 there is a broad peak in the 3289-2897 cm⁻¹ region, indicating the interaction between the O-H groups of Cs with PEG. A strong interaction between the -OH from the PEG group and the -NH2 and -OH groups of Cs is indicated by the expansion and lowering of spectral

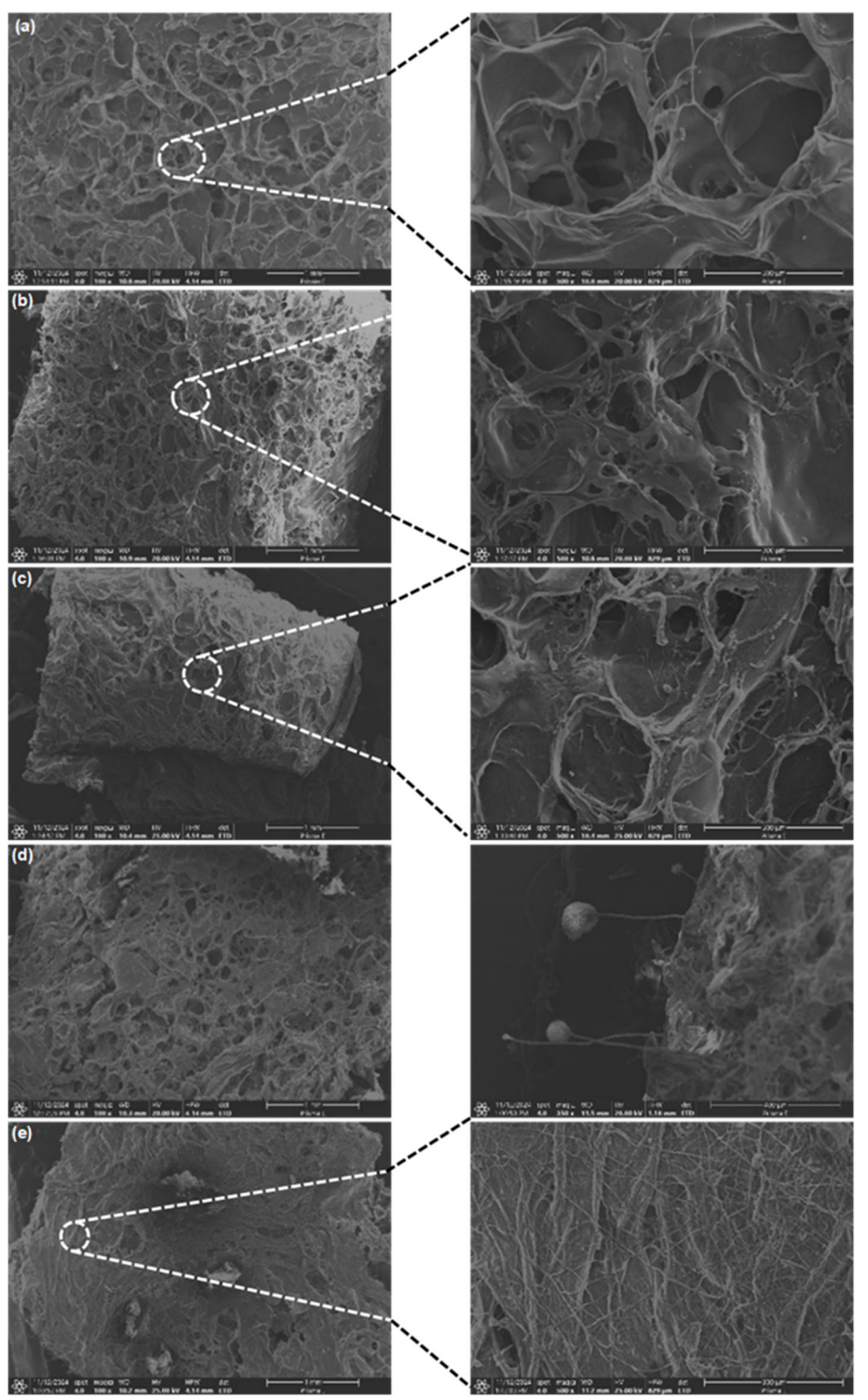


Fig 2. SEM image of hydrogel with zoom in 100 and 500 (a) F1, (b) F2, (c) F3, (d) F4, (e) F5. The dash line is a 500 magnification connector at a point of 100 magnification hydrogel

frequencies [7]. This occurs as a result of hydrogen bonds' attraction to O–H bonds and the dynamic modification of their spring constant. Strong evidence of intermolecular

interactions and superior molecular compatibility between Cs and PEG is shown by all of these alterations. Following interaction or attachment to the chitosan/PEG

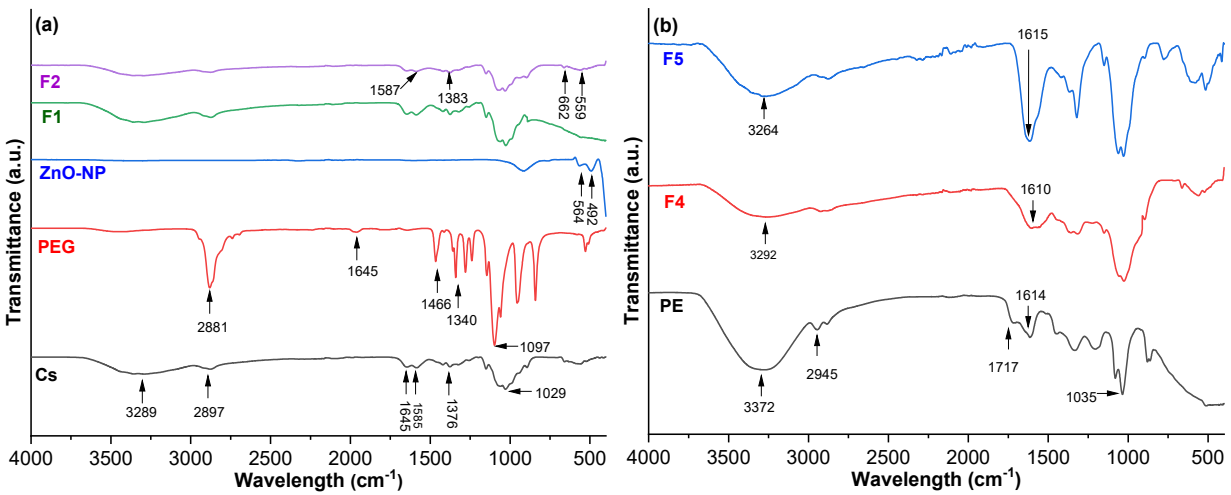


Fig 3. FTIR spectra of (a) Cs, PEG, ZnONP; F1 (Cs/PEG), and F2 (Cs/PEG/ZnO1), and (b) PE, F4 (Cs/PEG/ZnO1/PE), and F5 (Cs/PEG/ZnO4/PE)

network, the Zn–O strain mode shifts from 564 to 492 cm⁻¹, and the absorption bands at 662 and 559 cm⁻¹ in the Cs/PEG/ZnO spectra show the attachment of amine groups to ZnO-NP. ZnO-NP has a negatively charged surface, resulting in an electrostatic attraction force between ZnO-NP and the positively charged NH groups of Cs. These results are similar to research conducted by Masud et al. [7], where the addition of ZnO to the hydrogel gave rise to two typical ZnO absorption peaks at 629 and 536 cm⁻¹.

Another FTIR analysis was also performed on PE to determine its functional groups, as shown in Fig. 3(b). Specific signal of PE can be observed at 3372 (O-H stretch) which is characteristic of phenolic compounds in PE, 2945 (C-H stretch), 1717 (C=O stretch vibration), 1614 (C=C stretch vibration from aromatic rings), and 1035 (C–O stretch) cm⁻¹ which may come from alcohol or ether groups [42]. The addition of PE to the hydrogel resulted in a shift in the absorption band from 3292 to 3264 cm⁻¹, indicating the interaction of O–H groups from PE with the hydrogel matrix. The appearance of the absorption band at 1610 cm⁻¹ (F4) and 1615 cm⁻¹ (F5) is expected because the amino group (N-H) of Cs (amide II) interacts with the carbonyl group of PE through hydrogen bonding. Hosseini et al. [8] also experienced a shift in the absorption band due to the addition of PE. This is due to the penetration of PE in the hydrogel network

Swelling Test

Hydrogels have great potential for application in the pharmaceutical and medical industries because they have viscoelasticity and the capacity to hold large amounts of water, which makes them resemble living tissue. Furthermore, its high-water content promotes superior biocompatibility and quicker drug release [43-44]. The ability of hydrogel to absorb fluid can help maintain wound moisture, thereby accelerating cell migration. High swelling ability can increase the diffusion of active substances, thereby affecting the effectiveness of drug release in the wound area. Fig. 4 shows the swelling ratio of the hydrogel following a 24 h immersion in PBS solution (pH 7.4) at 37 °C. Maximum water absorption at F1, F2, F3, F4, and F5 was, respectively, 147.80, 113.85, 111.68, 134.42, and 126.08%. Swelling is influenced by crosslinking, hydrophilicity, and hydrophobicity of the polymer, temperature, solution pH, and other variables [45]. The swelling behavior of Cs in hydrogels depends on the ionic bonds between water molecules and Cs amino groups. Phosphate crosslinkers can also form hydrogen bonds with water and further increase water absorption. The chitosan amino group in this sample establishes an ionic interaction with the phosphate crosslinker after being protonated in an acidic environment. F1 has the highest water absorption rate. But, after adding ZnO to

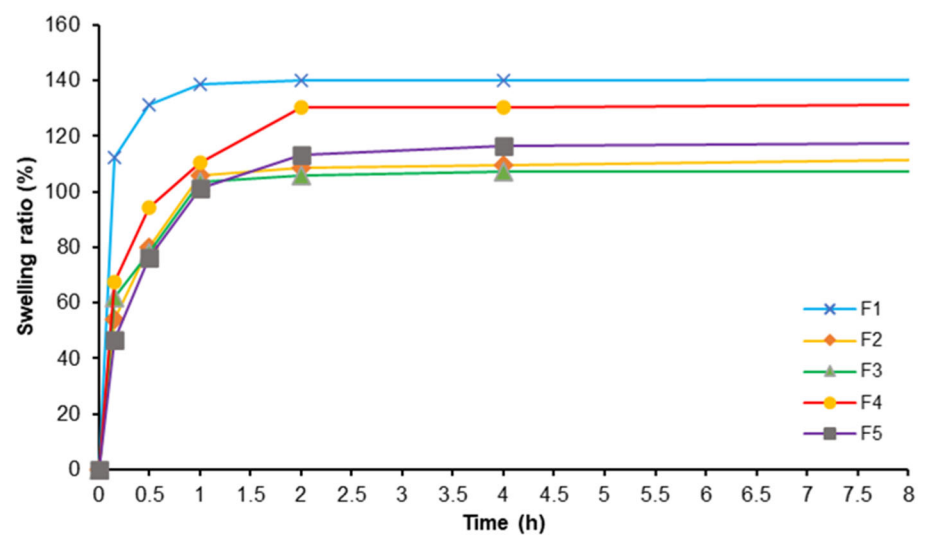


Fig 4. Swelling behavior of hydrogel in phosphate buffer saline (pH 7.4)

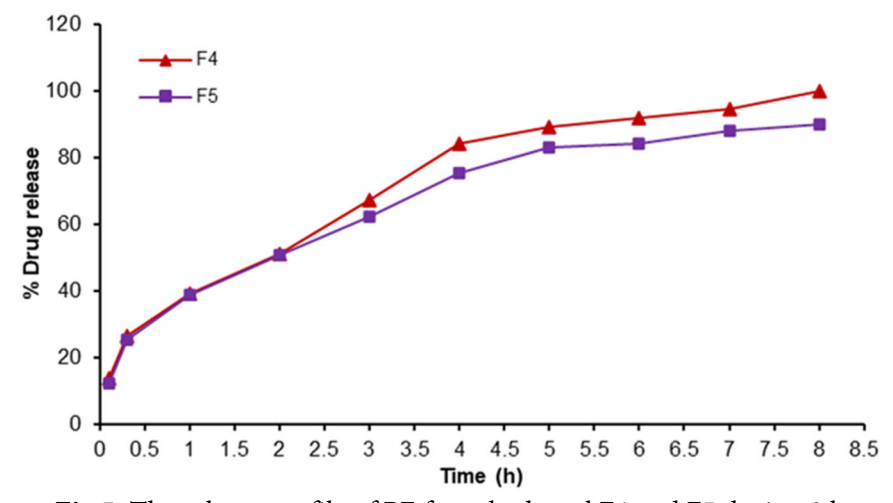


Fig 5. The release profile of PE from hydrogel F4 and F5 during 8 h

the hydrogel, the absorption capacity of the hydrogel decreased. This is caused by the interaction of ZnO with hydrogel functional groups (such as –OH, –NH₂ from Cs) thereby reducing the hydrogel's ability to absorb water. ZnO also has properties that are not completely hydrophilic, so more ZnO added can inhibit water absorption by the hydrogel. Similar results were also obtained in a study conducted by Rastegari et al. [46] where the addition of ZnO-NP to the hydrogel resulted in a decrease in the swelling ratio of the hydrogel.

Drug Release Study

Fig. 5 shows the release profile of the extract from the PE loaded samples. The best drug release speed

occurred at 1–4 h, where drug release occurred quickly, amounting to 62% (F4) and 67% (F5). This corresponds to the rapid swelling ability of the hydrogel at the beginning (the first 4 h), then the drug release slows down and tends to stagnate at 4–8 h. The drug release is also related to the result of the swelling test, where the higher the swelling value, the higher the drug release capacity. It can be seen in Fig. 5 (F4 and F5) where the swelling capacity of F4 is greater than F5, so the drug release in F4 is also greater then F5 (Fig. 5). In addition, there was also a tendency to decrease the drug release rate with increasing ZnO-NP concentration in the PEhydrogel. Similar results were also experienced by Rastegari et al. [46] where the addition of ZnO can

reduce the drug release profile. The hydrogen connection between ZnO-NP and PE, electrostatic interaction, and π - π stacking interaction are thought to be the causes of the decrease [8]. Based on these results, it shows that the release rate depends on the ZnO-NP content.

The drug release profiles of F4 and F5 were 100 and 89.89%, respectively, after 8 h of measurement at 37 °C in PBS (pH 7.4). Swelling, Cs chain breakdown, and PEG dissolution from the hydrogel into the medium can all cause drug molecules to be released from the hydrogel. This fast drug release is also due to the PEG content in the hydrogel. Upon coming into contact with PBS, the hydrogel's PEG content tends to break down, causing PE to be released [8].

Antibacterial Activity

The antibacterial activity of the hydrogel containing and not containing the PE was observed by measuring the zone of inhibition (Fig. 6(a)and (b)). Hydrogel with a ZnO content of 40 mg has the largest zone of inhibition for *E*.

coli and S. aureus bacteria, namely 16.24 and 16.94 mm, respectively. The hydrogel containing PE (F5) only has an inhibition zone of 10.64 and 6.54 mm. The main factor causing this is the chelation of ZnO-NP by bioactive compounds from plant extracts, which form a passive layer on the ZnO surface that will inhibit the release of Zn²⁺ ions and reduce antibacterial effectiveness [47]. This result is reinforced by the SEM morphology (Fig. 2(d)), which shows that the hydrogel with the addition of PE has denser pores compared to the hydrogel without PE, resulting in obstacles in the ZnO release process. The second possibility is the inhibition of the photocatalytic activity of ZnO, where bioactive compounds from plant extracts interfere with the photocatalytic activity of ZnO, which is needed to produce reactive oxygen species (ROS) as an antibacterial mechanism [48]. The inhibitory effect of ZnO on S. aureus is relatively stronger than E. coli. In line with research conducted by Xue et al. [49], ZnO-NPs

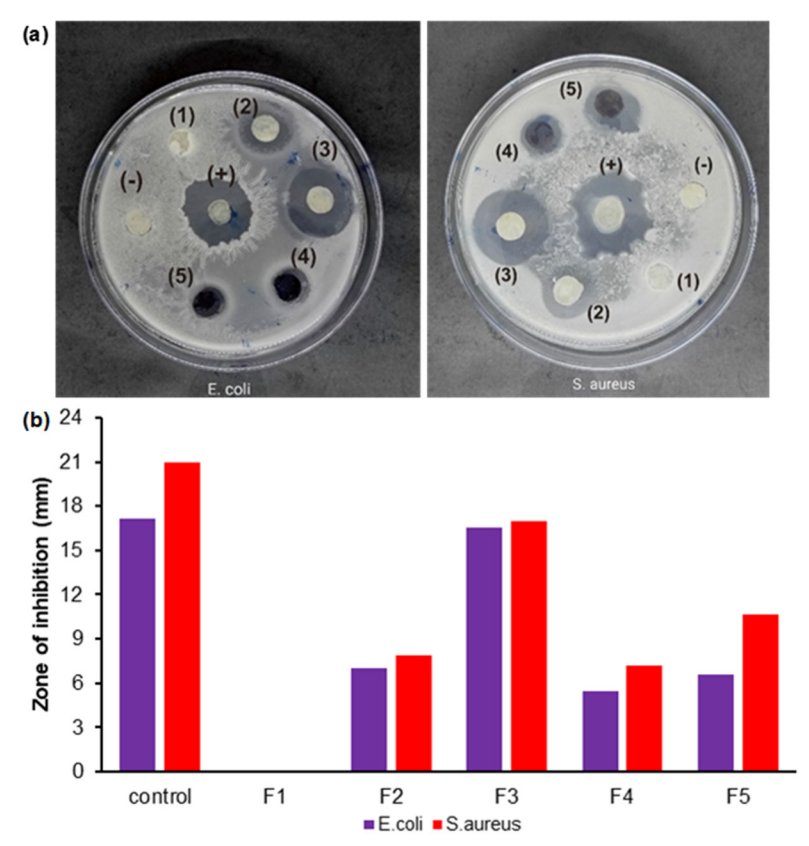


Fig 6. (a) Antibacterial activity of hydrogel containing ZnO and PE against *E. coli* and *S. aureus* bacteria; (b) comparison of inhibition zones

have a weak inhibitory effect against Gram-negative bacteria, such *as E. coli*, and stronger inhibition against Gram-positive bacteria, such as *S. aureus*.

In Vivo Analysis

Fig. 7(a) and (b) display the result of a 10-d experiment on a rat model to evaluate the hydrogel's capacity for wound healing. Wounds made in rats were covered with hydrogel containing PE, without PE, and 10% povidine iodine as a control. On day 5 after wounding, the formation of granulation tissue was clearly visible in rats wrapped with hydrogel, both with and without active substances. However, the hydrogel containing ZnO and PE showed faster wound closure compared to other treatments. Completely closed wounds were observed in wounds treated with hydrogel containing ZnO and PE after observation on the 10th day.

After observations, the resulting positive control wound (+) > F1 > F2 > F3 > F4 > F5diameter with respectively was 1.46, 1.11, 1.06, 0.94, 0.21, and 0.13 mm. In addition, skin treated with hydrogel containing PE appeared smoother and left fewer scabs compared to rats treated with other hydrogels and controls. The same results were obtained from the research conducted by Jokar et al. [50], where the addition of PE in the wound dressing component can accelerate the wound healing process in test animals. PE has strong antioxidant properties due to its soluble polyphenols. This helps protect cells from damage [51]. The main goal of antioxidants is to stop cell damage caused by free radicals coming into contact with cell membranes. These antioxidant components avoid ROS from increasing cell survival [52]. PE can stimulate fibroblast proliferation and production of collagen (COL-1) in large quantities

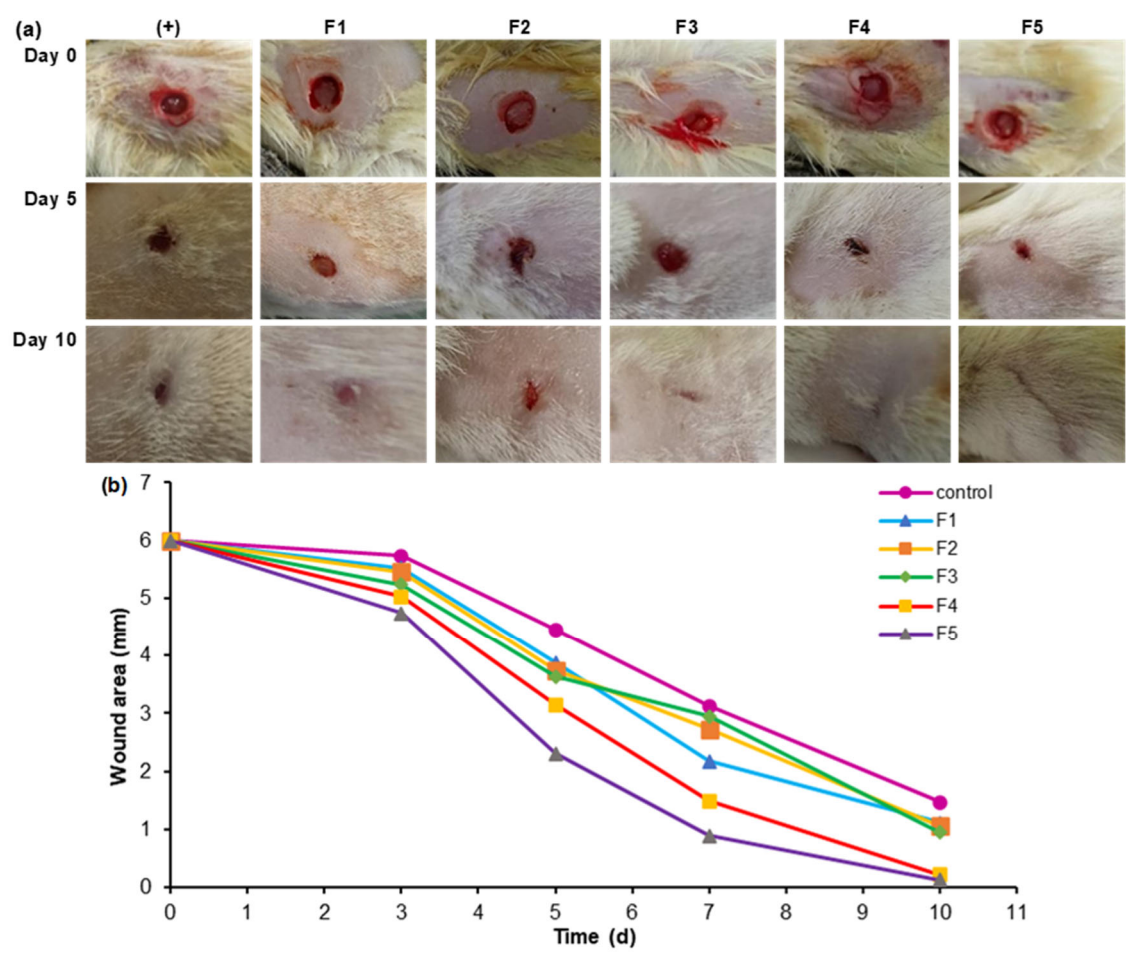


Fig 7. (a) Images of the wound healing process in mice treated with hydrogel and (b) graph of wound healing diameter after observation for 10 d

during the wound healing phase. The buildup and alignment of collagen in the healed area often indicate progress in wound healing [47-48].

CONCLUSION

This study used the solution mixing and casting approach to create a wound-healing hydrogels using Cs, PEG, ZnO-NP, and PE. XRD and DLS analysis confirmed that the co-precipitation method produced ZnO-NP that had high purity and nano size. The hydrogel showed the encapsulation efficiency of PE at 67% with a concentration of 20 mg/mL. FTIR analysis confirmed that the hydrogel contained ZnO and PE. From in vitro analysis, it was found that the hydrogel containing PE tended to weaken the antibacterial activity against E. coli and S. aureus. However, in vivo analysis it was observed that the hydrogel containing PE showed better wound healing properties than povidone iodine 10% and hydrogel without PE. With these results, it can be concluded that hydrogel with PE addition could be a potential candidate for biomedical applications, such as local medicine for soft tissue restoration

CONFLICT OF INTEREST

The authors declare that they have no known competing financial interests or personal relationships that could have appeared to influence the work reported in this paper.

AUTHOR CONTRIBUTIONS

All authors contributed equally to the manuscript, participated in this research, wrote, reviewed/edited, and approved the final draft for publication.

REFERENCES

- [1] Fadhil, I.A., Aldabbagh, B.M.D., and Mahdi, W.T., 2023, Preparing chitosan hybrid nanocomposites by novel additives for wound healing, *J. Polym. Compos.*, 11 (2), 9–23.
- [2] Sharmila, G., Muthukumaran, C., Kirthika, S., Keerthana, S., Kumar, N.M., and Jeyanthi, J., 2020, Fabrication and characterization of *Spinacia oleracea* extract incorporated alginate/carboxymethyl

- cellulose microporous scaffold for bone tissue engineering, *Int. J. Biol. Macromol.*, 156, 430–437.
- [3] Siahaan, P., Sasongko, N.A., Lusiana, R.A., Prasasty, V.D., and Martoprawiro, M.A., 2021, The validation of molecular interaction among dimer chitosan with urea and creatinine using density functional theory: In application for hemodyalisis membrane, *Int. J. Biol. Macromol.*, 168, 339–349.
- [4] Lusiana, R.A., Sangkota, V.D.A., Sasongko, N.A., Santosa, S.J., and Othman, M.H.D., 2019, Chitosan based modified polymers designed to enhance membrane permeation capability, *IOP Conf. Ser.: Mater. Sci. Eng.*, 509 (1), 012122.
- [5] Lusiana, R.A., Nuryanto, R., Muna, N., Dayanti, D., Gunawan, G., Kiswandono, A.A., Annisa, R.N., Septevani, A.A., and Sasongko, N.A., 2024, Highperformance sulfonated polyether sulfone/chitosan membrane on creatinine transport improved by lithium chloride, *Int. J. Biol. Macromol.*, 261, 129784.
- [6] Ghimire, S., Sarkar, P., Rigby, K., Maan, A., Mukherjee, S., Crawford, K.E., and Mukhopadhyay, K., 2021, Polymeric materials for hemostatic wound healing, *Pharmaceutics*, 13 (12), 2127.
- [7] Masud, R.A., Islam, M.S., Haque, P., Khan, M.N.I., Shahruzzaman, M., Khan, M., Takafuji, M., and Rahman, M.M., 2020, Preparation of novel chitosan/poly (ethylene glycol)/ZnO bionanocomposite for wound healing application: Effect of gentamicin loading, *Materialia*, 12, 100785.
- [8] Hosseini, S., Eslahi, N., and Jahanmardi, R., 2023, Self-healing nanocomposite hydrogels based on chitosan/modified polyethylene glycol/graphene, *Mater. Today Commun.*, 37, 107417.
- [9] Safitri, B., Hudiyanti, D., Laksitorini, M.D., Sasongko, N.A., and Siahaan, P., 2020, Intermolecular hydrogen bond interactions in Ncarboxymethyl chitosan and nH₂O: DFT and NBO studies, AIP Conf. Proc., 2237 (1), 020081.
- [10] Lusiana, R.A., Nuryanto, R., Dayanti, D., Khabibi, K., Wijayati, N., Sasongko, N.A., and Wijaya, A.R.,

- 2023, Synthesis and characterization of chitosan/polyvinyl alcohol immersed in sodium hydroxide thin film as a heterogeneous catalyst in biodiesel production, *Int. J. Biol. Macromol.*, 251, 126378.
- [11] Lusiana, R.A., Sangkota, V.D.A., Sasongko, N.A., Gunawan, G., Wijaya, A.R., Santosa, S.J., Siswanta, D., Mudasir, M., Abidin, M.N.Z., Mansur, S., and Othman, M.H.D., 2020, Permeability improvement of polyethersulfone-polietylene glycol (PEG-PES) flat sheet type membranes by tripolyphosphate-crosslinked chitosan (TPP-CS) coating, *Int. J. Biol. Macromol.*, 152, 633–644.
- [12] Seidi, F., Khodadadi Yazdi, M., Jouyandeh, M., Dominic, M., Naeim, H., Nezhad, M.N., Bagheri, B., Habibzadeh, S., Zarrintaj, P., Saeb, M.R., and Mozafari, M., 2021, Chitosan-based blends for biomedical applications, *Int. J. Biol. Macromol.*, 183, 1818–1850.
- [13] Lusiana, R.A., Indra, A., Prasetya, N.B.A., Sasaongko, N.A., Siahaan, P., Azmiyawati, C., Wijayanti, N., Wijaya, A.R., and Othman, M.H.D., 2021, The effect of temperature, sulfonation, and PEG addition on physicochemical characteristics of PVDF membranes and its application on hemodialysis membrane, *Indones. J. Chem.*, 21 (4), 942–953.
- [14] Lusiana, R.A., Sasongko, N.A., Sangkota, V.D.A., Prasetya, N.B.A., Siahaan, P., Kiswandono, A.A., and Dzarfan, M.H., 2020, In-vitro study of polysulfone-polyethylene glycol/chitosan (PEG-PSf/CS) membranes for urea and creatinine permeation, *J. Kim. Sains Apl.*, 8 (23), 283–289.
- [15] Raina, N., Singh, A.K., and Islam, A., 2021, "Biological Implications of Polyethylene Glycol and PEGylation: Therapeutic Approaches Based on Biophysical Studies and Protein Structure-Based Drug Design Tools" in *Innovations and Implementations of Computer Aided Drug Discovery Strategies in Rational Drug Design*, Eds. Singh, S.K., Springer Singapore, Singapore, 273–294.
- [16] Yadollahi, M., Farhoudian, S., Barkhordari, S., Gholamali, I., Farhadnejad, H., and Motasadizadeh, H., 2016, Facile synthesis of chitosan/ZnO bio-

- nanocomposite hydrogel beads as drug delivery systems, *Int. J. Biol. Macromol.*, 82, 273–278.
- [17] Liang, Y., He, J., and Guo, B., 2021, Functional hydrogels as wound dressing to enhance wound healing, *ACS Nano*, 15 (8), 12687–12722.
- [18] Sulaiman, R., Ghaffar, A., Preveen, S., Ashraf, D., Tariq, I., Kinza, K., and Shakir, T., 2023, Synthesis, characterization, and biomedical applications of zinc oxide nanoparticles, *BME Horiz.*, 1 (3), 89.
- [19] Ramesh, K., Ponnusamy, J., and Periasamy, P., 2024, Synthesis of antimicrobial and antioxidant zinc oxide hydrogel for drug delivery applications, *Indones. J. Chem.*, 24 (6), 1615–1627.
- [20] Gassim, F.A.Z.G., and Makkawi, A.J.J., 2023, Anticancer Activity of Synthesized ZnO and ZnO/AgCl Nanocomposites against Five Human Cancer Cells, *Indones. J. Chem.*, 23 (2), 333–340.
- [21] Emam-Djomeh, Z., and Hajikhani, M., 2023, "Chitosan/Poly (Ethylene Glycol)/ZnO Bionanocomposite for Wound Healing Application" in *Biodegradable and Environmental Applications of Bionanocomposites*, Eds. Visakh, P.M., Springer International Publishing, Cham, Switzerland, 31–65.
- [22] Prasad, A.S., and Bao, B., 2019, Molecular mechanisms of zinc as a pro-antioxidant mediator: Clinical therapeutic implications, *Antioxidants*, 8 (6), 164.
- [23] Gao, X., Xu, Z., Liu, G., and Wu, J., 2021, Polyphenols as a versatile component in tissue engineering, *Acta Biomater.*, 119, 57–74.
- [24] Qahir, A., Kakar, A.U.R., Khan, N., Samiullah, S., Hakeem, A., Kamal, R., and Ur-Rehman, F., 2021, The antioxidant, antimicrobial, and clinical effects with elemental contents of pomegranate (*Punica granatum*) peel extracts: A review, *Baghdad J. Biochem. Appl. Biol. Sci.*, 2 (1), 21–28.
- [25] Mo, Y., Ma, J., Gao, W., Zhang, L., Li, J., Li, J., and Zang, J., 2022, Pomegranate peel as a source of bioactive compounds: A mini review on their physiological functions, *Front. Nutr.*, 9, 887113.
- [26] Saigl, Z.M., and Ahmed, A.M., 2021, Separation of rhodamine B dye from aqueous media using natural

- pomegranate peels, *Indones. J. Chem.*, 21 (1), 212–224.
- [27] Purwaningsih, S.Y., Pratapa, S., Triwikantoro, T., and Darminto, D., 2016, Synthesis of nano-sized ZnO particles by co-precipitation method with variation of heating time, *AIP Conf. Proc.*, 1710 (1), 030040.
- [28] Gallas, J.A., Pelozo, L.L., Oliveira, W.P., Salvador, S.L., Corona, S.M., and Souza-Gabriel, A.E., 2023, Characterization, antimicrobial activity, and antioxidant efficacy of a pomegranate peel solution against persistent root canal pathogens, *Cureus*, 15 (8), e43142.
- [29] Safdar, M.N., Kausar, T., Jabbar, S., Mumtaz, A., Ahad, K., and Saddozai, A.A., 2017, Extraction and quantification of polyphenols from kinnow (*Citrus reticulate* L.) peel using ultrasound and maceration techniques, *J. Food Drug Anal.*, 25 (3), 488–500.
- [30] Lusiana, R.A., Protoningtyas, W.P., Wijaya, A.R., Siswanta, D., Mudasir, M., and Santosa, S.J., 2017, Chitosan-tripoly phosphate (CS-TPP) synthesis through cross-linking process: The effect of concentration towards membrane mechanical characteristic and urea permeation, *Orient. J. Chem.*, 33 (6), 2913–2919.
- [31] Shafiq, M., Yasin, T., Aftab Rafiq, M., and Shaista, S., 2013, Structural, thermal, and antibacterial properties of chitosan/ZnO composites, *Polym. Compos.*, 35 (1), 79–85.
- [32] Wang, L.C., Chen, X.G., Zhong, D.Y., and Xu, Q.C., 2007, Study on poly(vinyl alcohol)/carboxymethyl-chitosan blend film as local drug delivery system, *J. Mater. Sci.: Mater. Med.*, 18 (6), 1125–1133.
- [33] Bhowmik, S., Islam, J.M.M., Debnath, T., Miah, M.Y., Bhattacharjee, S., and Khan, M.A., 2017, Reinforcement of gelatin-based nanofilled polymer biocomposite by crystalline cellulose from cotton for advanced wound dressing applications, *Polymers*, 9 (6), 222.
- [34] Rowland, M.B., Moore, P.E., Bui, C., and Correll, R.N., 2023, Assessing wound closure in mice using skin-punch biopsy, *STAR Protoc.*, 4 (1), 101989.
- [35] Patra, P., Mitra, S., Debnath, N., Pramanik, P., and

- Goswami, A., 2014, Ciprofloxacin conjugated zinc oxide nanoparticle: A camouflage towards multidrug resistant bacteria, *Bull. Mater. Sci.*, 37 (2), 199–206.
- [36] Babayevska, N., Przysiecka, Ł., Iatsunskyi, I., Nowaczyk, G., Jarek, M., Janiszewska, E., and Jurga, S., 2022, ZnO size and shape effect on antibacterial activity and cytotoxicity profile, *Sci. Rep.*, 12 (1), 8148.
- [37] Clogston, J.D., and Patri, A.K., 2011, Zeta potential measurement, *Methods Mol. Biol.*, 697, 63–70.
- [38] Krishnakumar, V., and Elansezhian, R., 2021, Dispersion stability of zinc oxide nanoparticles in an electroless bath with various surfactants, *Mater. Today: Proc.*, 51, 369–373.
- [39] Khorasani, M.T., Joorabloo, A., Moghaddam, A., Shamsi, H., and MansooriMoghadam, Z., 2018, Incorporation of ZnO nanoparticles into heparinised polyvinyl alcohol/chitosan hydrogels for wound dressing application, *Int. J. Biol. Macromol.*, 114, 1203–1215.
- [40] Eichholz, K.F., Freeman, F.E., Pitacco, P., Nulty, J., Ahern, D., Burdis, R., Browe, D.C., Garcia, O., Hoey, D.A., and Kelly, D.J., 2022, Scaffold microarchitecture regulates angiogenesis and the regeneration of large bone defects, *Biofabrication*, 14 (4), 045013.
- [41] Wang, C., Feng, L., Yang, H., Xin, G., Li, W., Zheng, J., Tian, W., and Li, X., 2012, Graphene oxide stabilized polyethylene glycol for heat storage, *Phys. Chem. Chem. Phys.*, 14 (38), 13233–13238.
- [42] Safdar, M., Naqvi, S.A., Anjum, F., Pasha, I., Shahid, M., Waliullah, W., Jaskani, M.J., Khan, I.A., and Aadil, R.M., 2021, Microbial biofilm inhibition, antioxidants, and chemical fingerprints of Afghani pomegranate peel extract documented by gas chromatography–mass spectrometry and Fourier transformation infrared, *J. Food Process. Preserv.*, 45 (7), e15657.
- [43] Chamkouri, H., and Chamkouri, M., 2021, A review of hydrogels, their properties and applications in medicine, *Am. J. Biomed. Sci. Res.*, 11 (6), 485–493.
- [44] Maiz-Fernández, S., Pérez-Álvarez, L., Silván, U.,

- Vilas-Vilela, J.L., and Lanceros-Mendez, S., 2022, Photocrosslinkable and self-healable hydrogels of chitosan and hyaluronic acid, *Int. J. Biol. Macromol.*, 216, 291–302.
- [45] Mahmud, M., Daik, R., and Adam, Z., 2018, Influence of poly(ethylene glycol) on the characteristics of γ radiation-crosslinked poly(vinyl pyrrolidone)-low molecular weight chitosan network hydrogels, *Sains Malays.*, 47 (6), 1189–1197.
- [46] Rastegari, A., Hasanshakir, F., Mohammadi, Z., Saadatpour, F., Faghihi, H., and Moraffah, F., 2023, A chitosan-based hydrogel containing zinc oxide nanoparticles as a carrier for improving antibacterial activity and controlling the release of antibiotics, *Micro Nano Lett.*, 18 (7), e12172.
- [47] Mahlaule-Glory, L.M., Mbita, Z., Ntsendwana, B., Mathipa, M.M., Mketo, N., and Hintsho-Mbita, N.C., 2019, ZnO nanoparticles via Sutherlandia frutescens plant extract: Physical and biological properties, *Mater. Res. Express*, 6 (8), 085006.
- [48] Zhang, B., Yang, Z., Yang, S., Xu, Y., Tang, X., Mao, H., Dai, R., and Liang, X., 2024, Construction of ZnO/Cu₂O composites for enhanced antibacterial activity and analysis of antibacterial mechanism, *Inorg. Chem. Commun.*, 162, 112182.

- [49] Xue, J., Zhang, W., Wang, C., Zhu, L., and Cao, X., 2023, Preparation of nano-sized zinc oxide by adjusting the reaction system alkalinity and its antibacterial properties, *Funct. Mater.*, 30 (4), 620–624.
- [50] Jokar, F., Rahaiee, S., Zare, M., Nasiri kenari, M., and Mirzakhani, N., 2023, Bioactive wound dressing using bacterial cellulose/dextran biopolymers loaded with pomegranate peel extract: Preparation, characterization and biological properties, *J. Drug Delivery Sci. Technol.*, 84, 104461.
- [51] Sattariazar, S., Arsalani, N., and Nejad Ebrahimi, S., 2023, Biological assessment of synthesized carbon dots from polyphenol enriched extract of pomegranate peel, incorporated with *Mentha piperita* essential oil, *Mater. Chem. Phys.*, 294, 126981.
- [52] Savekar, P.L., Nadaf, S.J., Killedar, S.G., Kumbar, V.M., Hoskeri, J.H., Bhagwat, D.A., and Gurav, S.S., 2024, Citric acid cross-linked pomegranate peel extract-loaded pH-responsive β-cyclodextrin/carboxymethyl tapioca starch hydrogel film for diabetic wound healing, *Int. J. Biol. Macromol.*, 274 (Pt. 1), 133366.